Catalytic Oxidative Coupling of Methane
Heterogeneous or Homogeneous Reaction?

Hu, Lingjun; Pinto, Donato; Urakawa, Atsushi

DOI
10.1021/acssuschemeng.3c02088

Publication date
2023

Document Version
Final published version

Published in
ACS Sustainable Chemistry and Engineering

ACS Sustainable Chemistry & Engineering

pubs.acs.org/journal/ascecg

Research Article

Catalytic Oxidative Coupling of Methane: Heterogeneous or Homogeneous Reaction?

Lingjun Hu, Donato Pinto, and Atsushi Urakawa*

Cite This: *ACS Sustainable Chem. Eng.* 2023, 11, 10835−10844

Read Online

ACCESS | Metrics & More | Article Recommendations | Supporting Information

ABSTRACT: Direct valorization of methane via oxidative coupling of methane (OCM) is an encouraging alternative to conventional oil-based processes for the production of light hydrocarbons (ethane and ethylene). Abundant, inexpensive simple oxides such as MgO and La_2O_3 possess the ability to selectively activate methane. However, during OCM, the selective conversion to ethane and the following dehydrogenation to ethylene are threatened by the thermodynamically favored partial and total oxidation reactions to form CO and CO_2, respectively. With the aid of spatially resolved operando analysis of temperature and gas concentration along the catalytic bed, we demonstrate the relevance of highly exothermic reaction paths developed in the gas phase, i.e., the homogeneous reaction, during OCM conditions at the front of the catalytic bed, largely determining the total C_2 yield obtained on those systems. With the new insights provided by the analysis of temperature and concentration gradients along the bed, we redefine the positive effect of promoters (Li, Sr), which enhance the influence of catalyst surfaces. The effect of promoters is recognized in the suppression of the exothermic oxidation paths leading to undesired CO_x, thus limiting the formation of hotspots and driving the reaction toward the desired C_2 products.

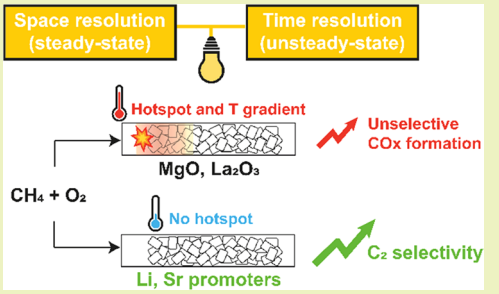

KEYWORDS: *oxidative coupling of methane, heterogeneous catalysis, operando spatial analysis, La_2O_3, MgO*

INTRODUCTION

Methane, the most abundant hydrocarbon in natural gas, is a potential candidate for the transition toward an oil-free chemical industry. Despite its abundancy, natural gas reservoirs are mainly located in remote regions and its price is still subject to multiple variables, including transportation infrastructure and political stability of the producing countries. In addition, until today, natural gas utilization has been limited to the generation of heat or a power source, contributing to global greenhouse gas emissions.[1] However, alternative and more valuable uses of methane are possible since it possesses a high potential to substitute oil in the synthesis of fundamental chemical commodities. Already industrially exploited is the production of hydrogen and syngas (CO + H_2) by steam reforming. Syngas can be further processed to target valuable products such as methanol or higher hydrocarbons through the Fischer−Tropsch process;[2] however, such multistep processes require higher investments to cope with the cost of transportation and storage.

Substantially more appealing is the opportunity to directly convert methane to added-value chemicals. Proposed strategies envisage the one-step conversion of methane to ethylene, methanol, formaldehyde, halogenated compounds, and aromatics.[3−6] Among these, the direct conversion of methane to ethylene is one of the most promising solutions, considering the market size of ethylene and its easier transportability in the liquid form. Also, this strategy would help speed up the decarbonization of the chemical industry. In fact, naphtha and ethane steam cracking are currently the main strategies for ethylene production. Energy demands of these processes are very high, resulting in high CO_2 emissions, up to 1.8−2 ton CO_2 per ton ethylene when naphtha is employed as the source.[7] The main challenge for the selective activation of methane is represented by the high energy required to break the first C−H bond of the molecule (439 kJ mol^{-1})[8] and initiate the reaction. The use of oxidants can help overcome the thermodynamic limitations linked to the activation of the stable C−H bonds in the methane molecule, as in the case of oxidative coupling of methane (OCM).[9]

The following reaction (Reaction 1) has attracted a lot of scientific interest with the promise of the one-step valorization of methane to ethylene.[10,11]

$$2CH_4 + O_2 = C_2H_4 + 2H_2O \quad \Delta H_{300K} = -281 \text{ kJ mol}^{-1} \tag{1}$$

It is commonly agreed that the reaction proceeds via formation of methyl radicals, usually requiring high temperatures of

Received: April 8, 2023
Revised: June 27, 2023
Published: July 14, 2023

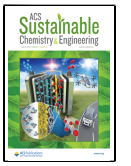

operation to be generated (600−800 °C).[4,12] Such radical species couple in the gas phase to form ethane, which is finally dehydrogenated to ethylene. The oxidative coupling of methane takes place in a complex reaction network where oxygen and highly reactive radical species, formed at high temperatures, are simultaneously present in the reactor.[13] From a thermodynamic point of view, partial and total oxidation products (CO_x) formation is favored in these conditions, limiting the total C_2 yield. In principle, heterogeneous catalysts can be utilized to kinetically drive the reaction toward the desired products, limiting the unselective routes. However, the minimum C_2 yield of 25−30%, estimated as a threshold to develop an industrially competitive ethylene production via OCM, has been only rarely approached.[14]

At the same time, complex catalyst formulations are frequently targeted to address higher catalytic performances, increasing the variables influencing the reaction network and mechanisms.[15] As a result, this complexity threatens the fundamental understanding of factors influencing OCM performances. A first step toward understanding the complexity of the OCM reaction network is to isolate the role of the catalyst in selectively activating CH_4 conversion. To do so, simple metal oxides represent model systems, which conveniently reduce the variables arising from complex catalytic systems. While providing high thermal and structural stability, such materials serve as oxidative templates on which CH_4 can be effectively activated.

Frequently employed along with promoters to enhance the catalytic properties, MgO and La_2O_3 possess a remarkable activity toward coupling products in OCM conditions. It is recognized that they contribute to the OCM reaction path, activating the methane molecule on their surface by abstraction of a hydrogen atom and generating a methyl radical.[16,17] The addition of alkali (Li) and alkaline-earth (Sr, Ba) metals as promoters is known to significantly enhance the OCM activity of simple metal oxides in terms of C_2 selectivity.[18,19] Literature reports on their effect on catalytic activity are abundant.[20,21] In general, it is agreed to correlate the positive trend of C_2 selectivity with properties such as the increased basicity and the increased lattice oxygen diffusivity introduced by the promoters.[22−25]

However, the fundamental role of simple oxides in promoting the selective conversion of methane into C_2 products is still under question. In OCM reaction conditions, the nature of the interaction of the metal oxides with CH_4 is masked by the presence of gaseous oxygen and the rise of exothermic reaction paths. Isolating the intrinsic activity of MgO and La_2O_3 toward CH_4 activation, in the absence of gaseous oxygen, can help elucidate the catalytic role of these oxides under OCM conditions.[26]

Great research efforts have been put into the definition of the reactions involved in the catalytic OCM, with the aim of deriving kinetic data and depicting a reaction mechanism. Nonetheless, individuating the fundamental properties governing the selectivity toward C_2 products remains challenging. The accuracy of the proposed kinetic models is threatened by the harsh conditions of OCM, which involve a complex chemical environment with a mixture of radical species, strong oxidants, and high temperatures of operation.[27,28] As for similar processes involving CH_4/O_2 mixtures, highly exothermic reactions are activated in an OCM reactor, resulting in the formation of hotspots.[13,29] This unavoidably leads to temperature and concentration gradients along the reactor bed, complicating the identification of the fundamental catalyst role and the individuation of the active sites that guarantee the selective conversion of methane.[30,31] These observations directly question the conventional approaches for catalytic studies, based on the mere interpretation of the reactor outlet composition and frequently ignoring the presence of temperature gradients. Instead, considering the influence of reaction temperature on the activation of methane[32] and oxygen,[33] it appears necessary to investigate the temperature and concentration profiles along the reactor bed in order to derive realistic insights into the OCM reaction.

In this work, we investigate the catalytic OCM by means of temperature and species concentration data spatially resolved along the reactor. Simple metal oxides (MgO, La_2O_3) are employed as basic catalytic systems, evaluating their intrinsic activity toward the selective activation of methane and their role played in OCM conditions. The contribution of the catalyst is discussed in light of the unique information about the temperature and concentration gradients developed in the reactor bed. With the same approach, the catalytic effect of promoters (Li-promoted MgO, Sr-promoted La_2O_3) in the OCM reaction is also investigated in light of the new insights derived from spatially resolved analysis.

EXPERIMENTAL SECTION

Catalyst Preparation. MgO (≥99% trace-metal basis, Sigma-Aldrich) and La_2O_3 (99.99%, Alfa Aesar) were used as simple metal oxide catalysts without any further treatment. The doped catalysts were prepared via a direct solid mixing method. The simple metal oxides and corresponding dopant metal carbonate salts ($SrCO_3$ for La_2O_3 and Li_2CO_3 for MgO) were mixed in an agate mortar with a certain amount of deionized water (1 mL of water per gram metal oxide). After that, the slurry was dried in an oven at 80 °C for 12 h and then calcined in a furnace at 800 °C for 4 h.

Catalyst Characterization. Power X-ray diffraction (PXRD) was performed on a D8 Advanced powder diffractometer (Bruker), with a germanium monochromator for Cu Kα1 radiation (λ = 1.5406 Å), at a scan step of 0.02°/s from 10 to 80°.

Catalytic Testing. 200 mg of catalyst material (pelletized, crushed, and sieved to the size range of 300−400 μm) was loaded into a quartz tube reactor, fixed between quartz wool layers. La_2O_3 was pretreated in O_2 (50 vol % in He, 50 mL/min) at 700 °C for 30 min before the reaction, considering the high tendency of La_2O_3 to form hydroxides upon exposure to moisture in air (see Figure S1 and Supporting Information S3).[34]

The reaction setup is illustrated in Scheme S1 (Supporting Information S1). It consists of three parts: gas controlling, reactor part, and gas analysis. For the first part, four different gases (He, O_2, N_2, CH_4) are connected to a system of two 4-way switching valves controlled by software. By changing the position of two 4-way switching valves, two modes of operation are available: steady-state operation and unsteady-state operation. For steady-state operation, a reactant mixture of CH_4 (40 vol %), O_2 (10 vol %), N_2 (13 vol %), and He (rest, 37 vol %) with a total flow rate of 80 mL/min was introduced into the reactor. The temperature of the catalytic bed was controlled by a Watlow heating control with a thermocouple inserted in the reactor and positioned at the end of the bed. The composition of the exhaust gas was analyzed by gas chromatography (GC, Agilent 7890B, equipped with two FID and one TCD) after passing through a small water condenser cooled by water circulation. For the experiment studying the effect of H_2, 1.5 vol % H_2 was added into the feed and the N_2 volume portion was reduced to 11.5%. For the unsteady-state catalytic reaction, alternation of the gaseous mixtures (CH_4, He, and 25 vol % O_2 in He) was implemented by a system of two 4-way switching valves controlled by software. The gas introduced into the reactor follows the following sequence: 25 vol % O_2 in He−pure He−

https://doi.org/10.1021/acssuschemeng.3c02088
ACS Sustainable Chem. Eng. 2023, 11, 10835−10844

pure CH_4−pure He, with the flow rate of 50 mL/min for each gas. Multiple cycles were conducted for each catalyst. The exhaust gas was analyzed by a combination of Fourier transform infrared (FTIR) spectroscopy (Bruker α) and mass spectrometry (Omnistar Pfeiffer Vacuum), and the presented results were the average of multiple stable cycles.

Spatial Analysis and Visual Inspection. For the temperature and catalyst bed visualization, the reactor furnace cover was modified by opening a ca. 3 cm × 1 cm window and the window was covered with a glass plate to avoid heat loss. A USB digital microscope (800−1000× magnification) was used to visually observe color changes of the catalyst bed and particles. An infrared camera (Micro-SWIR 320CSX camera, Sensors Unlimited) was used to take infrared (IR) radiation images that were converted to variations of temperature upon calibration. Details of space-resolved gas sampling and temperature measurements are provided in the Supporting Information.

RESULTS AND DISCUSSION

Unsteady-State Oxidative Coupling of CH_4. The intrinsic activity of MgO and La_2O_3 toward CH_4 activation was investigated by an unsteady-state catalytic reaction performed at different temperatures by alternation of O_2 (25 vol % in He) and pure CH_4 pulses separated by a He purge.

A temperature of 900 °C was necessary to observe C_2 products, while CO and H_2 production could already be detected at 700 °C. Figure 1 reports the product distribution obtained during exposure of La_2O_3 and MgO to the CH_4 pulse at 900 °C. In the absence of gaseous oxygen, the total oxidation of CH_4 to CO_2 was strongly suppressed, as indicated by the absence of the CO_2 signal below the detection limit (order of 100 ppm). At the same time, both catalysts were able to supply oxygen species from the lattice for the activation of CH_4. This finding indicates a high selectivity of lattice oxygen as an oxidant, in accordance with other transient experiments.[35,36]

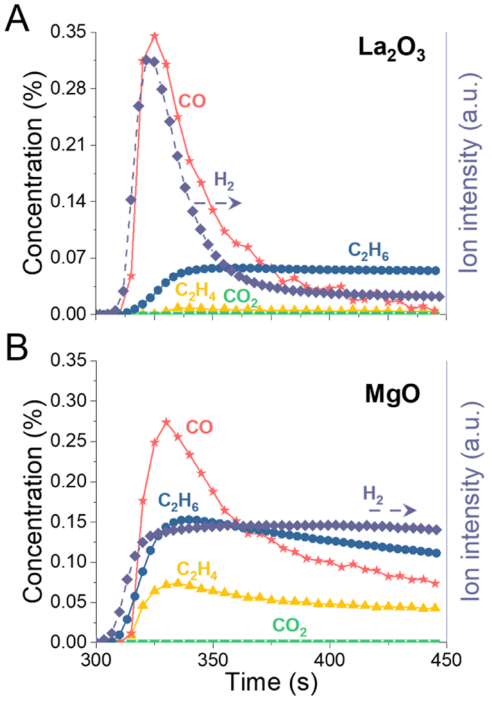

Figure 1. Concentrations of C_2H_6, C_2H_4, CO_2, and CO and ion intensity of H_2 (m/z = 2) in the CH_4 pulse during OCM under unsteady-state operation on La_2O_3 (A) and MgO (B) at 900 °C. C_2H_4, CO_2, and CO concentrations are quantified by IR and the C_2H_6 concentration is quantified by mass spectrometry data, which are calibrated with a simultaneous gas chromatography analysis. The values are averaged over multiple stable cycles of operation.

MgO presents an intrinsic ability to activate methane and promote its dehydrogenation reactions, while participation of lattice oxygen species to the partial oxidation of CH_4 to CO takes place at a relatively slow rate compared to rare-earth metal oxides. Constant H_2 production, extensive coking, and formation of C_2H_4 are products of dehydrogenation reactions involving CH_4 and C_2H_6.

The ability of MgO to provide lattice oxygen for reactions was already demonstrated by isotopic transient kinetics studies, which revealed oxygen exchange from the surface layers of MgO.[37] This limited reducibility, probably circumscribed to the surface of the oxides, is a key property to balance between CH_4 activation and its selective oxidation. The present results show that MgO possesses a unique intrinsic selectivity toward coupling products (Figure 1B). This superiority is often correlated to the high basicity of alkaline-earth metal oxides.[23,38] In contrast, La_2O_3 manifested high initial activity toward the partial oxidation of methane, as indicated by the matching peaks of CO and H_2 produced in the CH_4 pulse (Figure 1A). La_2O_3 is known for its high activity in producing gas-phase methyl radicals.[39] However, in the absence of gaseous oxygen, only limited C−C coupling ability is demonstrated. In rare-earth metal oxides, the prominent selectivity for partial oxidation products may derive from the reducibility of surface oxygen species, which can actively participate in the conversion of methane.[40] In the case of La_2O_3, the high initial partial oxidation activity is abruptly lost, indicating quick deactivation of the catalytic surface, possibly by carbon deposition, somehow affecting the accessibility of lattice oxygen for the selective oxidation of methane to CO.

To further investigate the different behavior of the MgO and La_2O_3 catalytic system, transient analysis of products evolved during unsteady-state CH_4 oxidation experiments is reported in Figure 2. Besides pure MgO and La_2O_3, two catalytic beds are prepared with a mixture of simple oxides. In one configuration, a mixed bed containing equal amounts of the two simple oxides is loaded (50 wt % La_2O_3, 50 wt % MgO, physical mixture). In the other configuration, a layer of La_2O_3 is placed in front of a MgO catalytic bed (10 wt % La_2O_3, 90 wt % MgO), preventing mixing of the two oxides.

The results obtained for the 50 wt % physical mixture of the two catalysts reveal that CO and H_2 releases are highly enhanced in this configuration. From a mechanistic point of view, these results confirm the intrinsic catalytic behavior observed for the pure catalysts: on the one hand, the ability of MgO in methane activation and dehydrogenation and, on the other hand, the high reactivity of the oxygen species in La_2O_3 to promote partial oxidation to CO. The MgO surface is very active for the activation of CH_4 and $CH_3^{\bullet}$ radicals formation. However, in a pure MgO catalytic bed, the absence of highly reactive O species in the lattice limits their further oxidation to CO. The presence of La_2O_3 in the catalytic bed introduces this highly reactive oxygen species, which promotes the oxidation of CH_4, C_2H_6, and the respective methyl and ethyl radicals formed on MgO, resulting in the decrease of C_2 species and a highly increased CO production compared to the pure MgO case.

To investigate the extent of coking, Figure 3 reports the profiles of CO_x species evolved from gasification of the carbon

https://doi.org/10.1021/acssuschemeng.3c02088
ACS Sustainable Chem. Eng. 2023, 11, 10835−10844

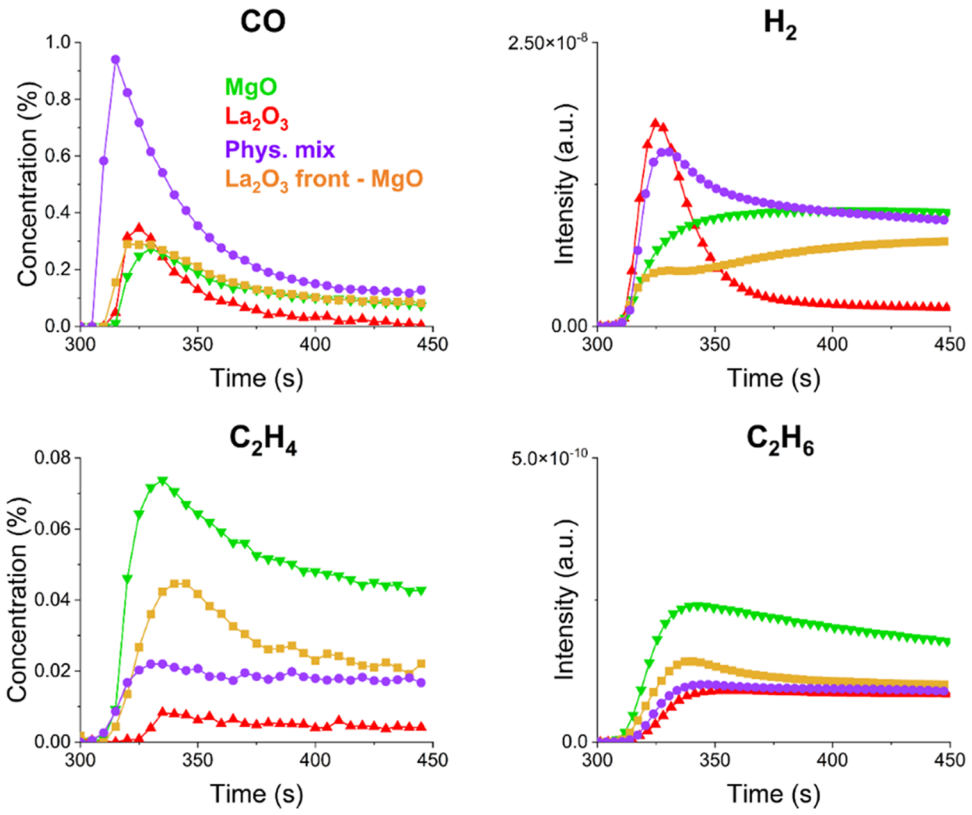

Figure 2. Transient analysis of products (FTIR + MS) during the CH_4 pulse (300−450 s) in unsteady-state OCM performed at 900 °C. The values are averaged over multiple stable cycles of operation. Results for La_2O_3 (red ▲), La_2O_3-MgO 50 wt % physical mixture (violet ●), MgO (green ▼), and La_2O_3 (10 wt %, front of the bed)-MgO (yellow ■).

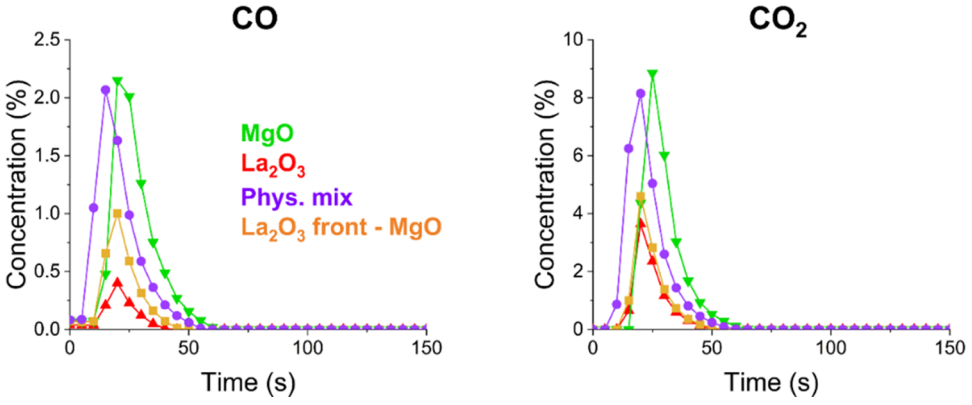

Figure 3. Transient analysis of products (FTIR + MS) during the O_2 pulse (0−150 s) in unsteady-state OCM performed at 900 °C. The values are averaged over multiple stable cycles of operation. Results for La_2O_3 (red ▲), La_2O_3-MgO 50 wt % physical mixture (violet ●), MgO (green ▼), and La_2O_3 (10 wt %, front of the bed)-MgO (yellow ■).

deposits during the oxidant pulse (O_2, 25 vol % in He). Pure La_2O_3 exhibited the lowest C deposition, while the highest accumulation of C deposits was found on MgO. For the 50 wt % mixture of MgO and La_2O_3, it would be reasonable to expect an amount of C deposited per g of catalyst close to the average value of the pure oxides. Interestingly, for the 50 wt % mixture of MgO and La_2O_3, CO_x species were released in a comparable amount to the pure MgO catalytic bed. It is clear that, in the presence of La_2O_3, the mechanism of carbon deposition proceeded unaltered on the MgO surface, confirming the high dehydrogenation activity of the catalyst.

A possible explanation for the high value of the CO_x species found in the mixed catalytic bed is the presence of a concentration gradient, with a preferential accumulation of carbon deposits at the front of the reactor bed. To verify this, a catalytic bed was prepared by loading a limited amount of La_2O_3 at the front of the MgO catalytic bed (La_2O_3 10 wt %, MgO 90 wt %, 200 mg). For this catalytic bed, the synergy observed for the physically mixed bed (50 wt %) disappears. In fact, the separate contribution of the two catalysts can be recognized in the transient product profiles (Figure 2). The small amount of La_2O_3 at the front of the catalytic bed is responsible for the initial higher peak observed in CO and H_2 profiles. The rest of the bed, composed of MgO, is mainly responsible for the C_2 production and the continuous H_2 generation from dehydrogenation reactions. The absence of

https://doi.org/10.1021/acssuschemeng.3c02088
ACS Sustainable Chem. Eng. 2023, 11, 10835−10844

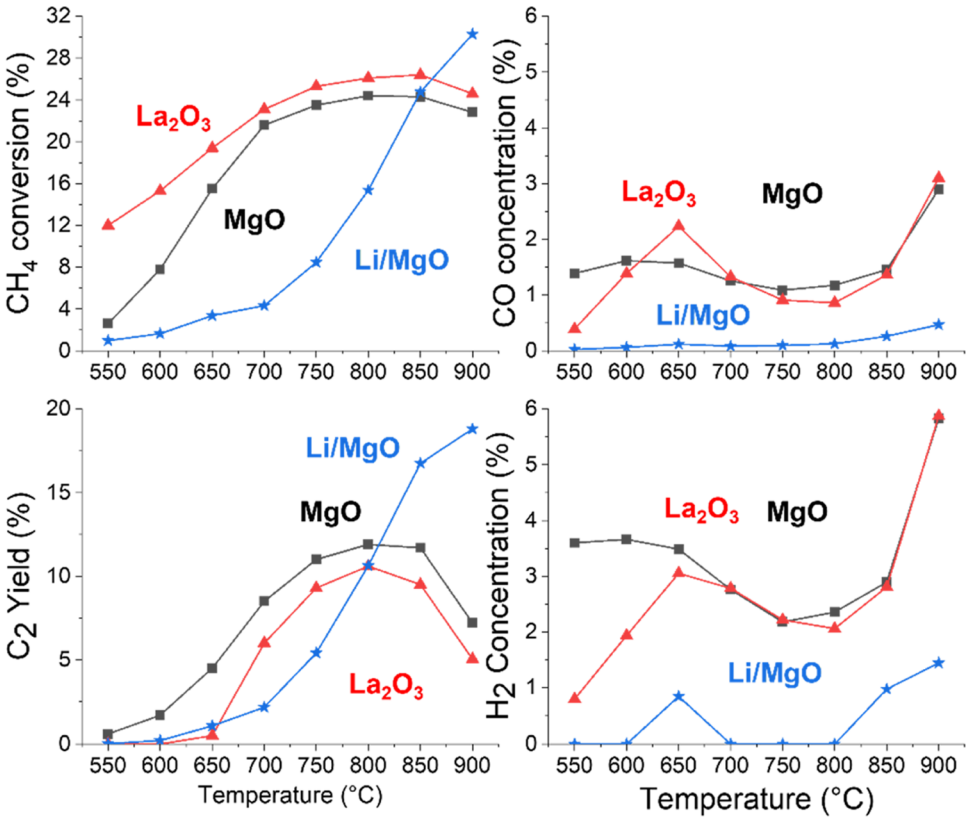

Figure 4. Catalytic performance of MgO (black), La_2O_3 (red), and 5 wt % lithium-doped MgO (Li/MgO, blue) in terms of CH_4 conversion (A), CO concentration (B), C_2 yield (C), and H_2 concentration (D) during OCM under steady-state operation (CH_4/O_2 = 4, 80 mL/min, He and N_2 diluted, N_2 is the internal standard for gas chromatography analysis) at different temperatures.

La_2O_3 particles in close vicinity allows the methyl radicals, generated on the MgO surface, to couple in the gas phase and form C_2H_6, without undergoing further oxidation to CO.

The reduced amount of MgO in the catalytic bed was reflected in the lower production of C_2 species, although the reduction clearly exceeded 10%, indicating that the front part of the catalytic bed may be responsible for the high share of the CH_4 conversion. Operando visualization of the catalytic bed (Supporting Information S4 and Figure S2) revealed that, at the end of the CH_4 pulse, the La_2O_3 catalyst placed at the front maintained its white color due to its resistance to carbon deposit formation, while MgO turned into a dark-gray color, indicating formation of carbon deposits. However, the presence of La at the front of the catalytic bed also strongly suppressed the total carbon deposition, as observed in the amount of CO_x species developed in the O_2 pulse (Figure 3). The results suggest the relevance of possible concentration gradients in the conversion of CH_4 and confirm the preferential accumulation of C at the front of the catalytic bed.

Steady-State Oxidative Coupling of CH_4. The unsteady-state investigation of the catalyst interaction with methane indicated peculiar selective conversion paths for the two oxidic systems. However, such prominent differences in the intrinsic catalytic behavior are severely lost in steady-state OCM operation.

The catalytic activity of simple metal oxides, La_2O_3 and MgO, was evaluated by quantifying the gaseous concentration in the reactor outlet during OCM operation at different temperatures. The catalytic activity of La_2O_3 was found to be superior to that of MgO in terms of CH_4 conversion and C_2 yield (Figure 4A,C), more prominently at lower temperatures (550−650 °C). In such conditions, remarkably higher amounts of partial oxidation products (CO and H_2, Figure 4B,D) were detected for La_2O_3, reflecting what was observed for the unsteady-state catalytic results (Figure 1A). However, the higher activity toward C_2 products compared to MgO contrasts the consideration on the intrinsic selectivity of the oxides.

Even more strikingly, the two materials behaved similarly above 700 °C. The catalytic activities of the two systems were comparable in terms of conversion and selectivity, and a similar trend of decrease in catalytic performance above 850 °C is observed. The concentration of CO_2 also confirmed these trends (Supporting Information S5 and Figure S3).

In this temperature range, O_2 is almost fully consumed and CH_4 total and partial oxidation products are detected at similar levels (Figures 4 and S3). This is an indication that reactions may be driven fully homogeneously and unselective exothermic reaction paths leading to CO_x species formation became predominant irrespective of the catalytic system. This given, it appears crucial to identify the extent of exothermic reaction paths for the two systems by investigating the distribution of heat in the catalytic reactor under reaction conditions.

Temperature and Concentration Gradients. A digital microscope and an infrared camera were used to qualitatively and quantitatively evaluate the temperature distribution along the catalytic bed. Remarkably, clear hotspots were observed (Figure 5A,B) only at the front of the catalyst bed for both catalysts. To evaluate the temperature in the inner part of the reactor, additional spatial temperature measurements were performed using a movable thermocouple inserted in the catalytic bed (Figure 5C). The measurements suggested that the temperature rise starts even before the catalyst bed,

https://doi.org/10.1021/acssuschemeng.3c02088
ACS Sustainable Chem. Eng. 2023, 11, 10835−10844

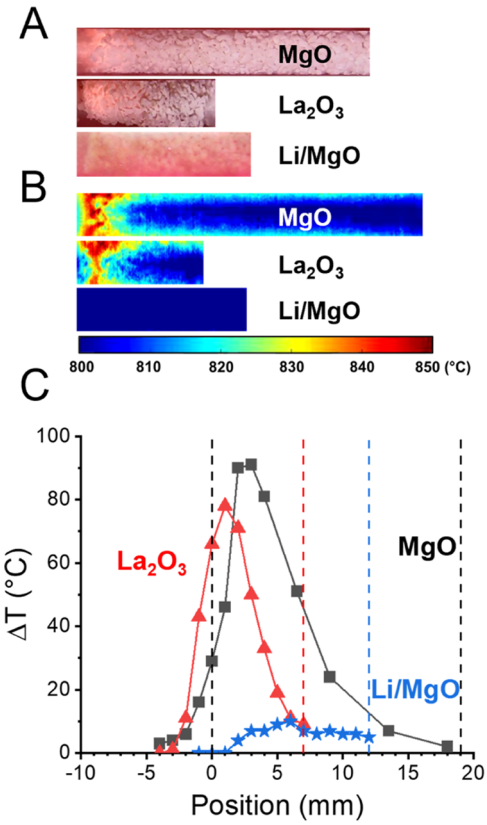

Figure 5. Visualization and quantification of hotspots formed during OCM under steady-state operation on MgO and La_2O_3, respectively, at 800 °C: (A) images of catalyst beds obtained by the digital microscope; (B) images of catalyst beds acquired via the infrared camera; (C) spatial distribution of the differential temperature of the catalyst (ΔT). The temperature rise is calculated by subtracting the temperature measured with 10 vol % O_2 in N_2 at 800 °C from the temperature measured during OCM under steady-state operation (the same feed composition as in Figure 4) at 800 °C at respective positions on corresponding catalysts.

although differences in heat conductivity make a precise delimitation of the hotspot challenging. Nonetheless, the hot zone in La_2O_3 appeared to be shifted more to the front of the catalyst bed compared to that of MgO, indicating that the exothermic reactions might be activated at an earlier position for La_2O_3.

Considering the presence of hotspots in OCM conditions, it is necessary to investigate possible gradients in the product distribution along the catalytic bed. To this end, space-resolved gas sampling was performed for the two catalysts. The profiles obtained during OCM at 700 °C are presented in Figure 6A,B.

The concentration profiles of oxygen clearly indicate that most of the oxygen is consumed within a few mm from the front edge of the catalyst bed of MgO and La_2O_3 (note that the catalyst bed length of La_2O_3 is significantly shorter because of its higher mass density). There is residual oxygen present in the reactor toward the end of the catalyst bed for La_2O_3 (Figure 6B). Nevertheless, only looking at the oxygen profiles, it is evident that the reactions take place mainly at/near the front position of the catalyst bed in accordance with the temperature profiles (Figure 5) and with other spatial gas analyses.[30,41,42] In practice, the localized reaction zone does not seem to affect the OCM performance positively and rather it can be detrimental, as evidenced by the decay of the C_2H_6

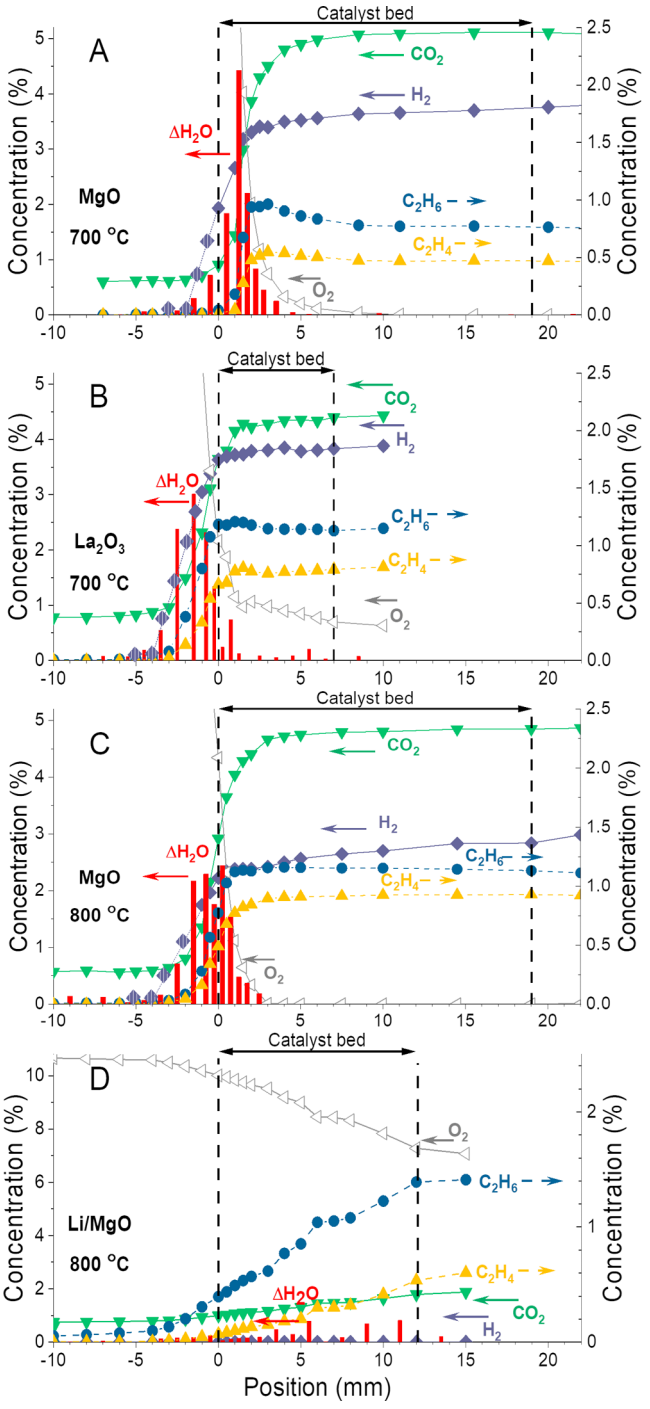

Figure 6. Space-resolved concentration profiles of CO_2, O_2, C_2H_6, C_2H_4, H_2, and formed water between two data points (ΔH_2O) measured during OCM under steady-state operation on (A) MgO at 700 °C, (B) La_2O_3 at 700 °C, (C) MgO at 800 °C, and (D) Li/MgO at 800 °C (same feed composition as in Figure 4).

and C_2H_4 concentrations after the initial peak values near the front of the catalyst bed. When using a lower amount of MgO in the catalytic bed (40 mg instead of 200 mg), no significant change in the catalytic activity toward C_2 products was observed (Supporting Information S5 and Figure S4). This result evidences that only a small portion of the catalyst at the front position positively contributes to OCM. Looking at the spatially resolved concentration profiles of OCM on MgO at 850 °C, the decrease of the C_2H_6 concentration along the bed

https://doi.org/10.1021/acssuschemeng.3c02088
ACS Sustainable Chem. Eng. 2023, 11, 10835−10844

is accompanied by the increase of CO and H_2, suggesting that reforming reactions can take place and negatively affect the total C_2 yield along the catalytic bed (Figure S5).

To our great surprise, the reaction products appear in the gas phase even before the catalyst bed, with a more pronounced phenomenon observed in La_2O_3 than MgO at 700 °C. This observation was also reported for MgO when the reaction temperature was increased to 800 °C (Figures 6C and S6A,B). Back-diffusion of products and gas mixing may be at the origin of this phenomenon. In order to check these influences, SiC was added before the catalyst beds. The concentration profiles (Figure S7) confirm an identical observation, with an even more pronounced shift of the products toward the inlet direction, possibly due to the higher gas temperature induced by the presence of heated SiC at the inlet position of the catalyst.

These observations pose fundamental questions on the role of the catalyst in OCM. The catalyst is undoubtedly necessary since inert materials as SiC cannot efficiently catalyze OCM (Figure S8). As noted above, the presence of products before the bed was more prominently observed for La_2O_3. All products reached their maximum concentration values in the catalyst-free zone even at 700 °C. A careful comparison of the gas-phase concentrations of the detected molecules indicates that the H_2 concentration profile was significantly distinct from the others and H_2 was observed at a much earlier point along the flow direction. Given the Maxwell−Boltzmann distribution, lighter molecules such as H_2 are in fact expected to back-diffuse faster at higher temperatures, explaining why H_2 was found at earlier positions before the catalytic bed. Here, the copresence of H_2 and unreacted O_2 from the feed created the conditions for additional highly exothermic reactions, such as CH_4 and H_2 oxidation, to take place and to cause the formation of local hotspots. The analysis of the H_2O produced at different positions in the catalyst bed (Figure 6, red bars) suggests that increased H_2O detection was also associated with an increment in the formation of other products, including C_2 species (Figure 6). In fact, the increased temperature is known to enhance the rate of the homogeneous gas-phase reactions in OCM.[43] In line with indications from homogeneous gas-phase OCM experiments, also the formation of C_2 products becomes relevant at T higher than 800 °C.[44] Due to the highly exothermic reaction pattern, the reaction mixture was locally heated up significantly, probably at least by a few hundred degrees (the exact determination of the temperature profile measurement is limited by the spatial resolution of the thermocouple or IR camera), and unselective oxidation reactions took place in the gas phase. A complex homogeneous reaction network involving several radical species (H, OH, CH_3) is expected to control the distribution of products.[45]

Still, the production of H_2 itself reflects the role played here by the catalyst. As discussed previously, H_2 can be produced from partial oxidation and the lattice oxygen in the La_2O_3 can more efficiently catalyze the reaction (Figure 1). This is in agreement with the observation from the unsteady-state: at the front edge of the catalyst bed (at 0 mm), 3.6 vol % H_2 was observed for La_2O_3, which was almost double the value observed for MgO (1.9 vol %) at 700 °C (Figure 6). The higher concentration of H_2 produced by La_2O_3 also explains its increased back-diffusion at the front of the bed. A higher concentration gives a larger diffusion driving force, enhancing H_2 back-diffusing further away from the La_2O_3 catalyst bed. Moreover, the exothermicity of the partial oxidation reaction and the heat generated by concomitant hydrogen oxidation are expected to provoke gas expansion, contributing to the back-diffusion phenomenon. The presence of H_2 and the consequent exothermic oxidation routes developed positively influence the yield of OCM products. Such an effect was confirmed by adding 1.4 vol % H_2 into the OCM feed using SiC, La_2O_3, or MgO as the catalyst (Figure S9). Additional support to those hypotheses was provided by an experiment where a small portion of La_2O_3 was placed in front of MgO. In this case, La_2O_3 would generate more H_2, and MgO may efficiently catalyze OCM. As expected, we could confirm the significant enhancement of catalytic performance in this configuration of the catalyst compared to MgO (Figure S10).

It is clear that the function of the catalyst is to catalytically trigger the reaction by first activating methane on its surface. The local hotspots generated by highly exothermic reactions, including H_2 oxidation, provoke the activation of homogeneous gas-phase reactions, which greatly control the product distribution. In such conditions, the majority of the reactions take place at the front of the catalyst bed, where oxygen is fast depleted. The higher activity of La_2O_3 over MgO at lower temperatures is attributed to the higher amount of H_2 produced by the former. However, the amount of produced H_2 seems to reach a similar level above a certain temperature (700 °C), indicating that, above this temperature, the specific impact of the metal oxide loses relevance in favor of the homogeneous gas-phase reaction steps, explaining the similar activity and trends (Figure 4).

Catalytic Effect of Promoters. In OCM studies, it is common to add promoter(s)/dopant(s) to simple metal oxides to improve the catalytic activity.[12] In light of the previous insights about the role of simple metal oxides in OCM reaction conditions, it is now possible to investigate the catalytic effect of promoters in terms of the spatial variation of product distribution and temperature. Figure 4 shows the catalytic performance of Li/MgO, which differs significantly from that of MgO. At first sight, the promotional effect of Li seems to be related to the lower activity of the catalyst toward CH_4 conversion in the lower temperature range (550−750 °C). However, CH_4 conversion and C_2 yield increase as the reaction temperature increases, in contrast to the trend observed in MgO (and La_2O_3). At the maximum temperature examined (900 °C), higher CH_4 conversion was observed for the Li-promoted sample compared to MgO, together with enhanced C_2 yield mainly due to the suppression of unselective oxidation reactions (CO and CO_2 formation, Figure S3).

An identical space-resolved concentration analysis was performed for Li/MgO at 800 °C (Figure 6D), clarifying the drastic differences in the spatial profiles of the gas-phase species in the reactor. The amounts of detected H_2 as well as H_2O were negligible, indicating that the addition of lithium greatly suppresses H_2 formation and, consequently, its exothermic oxidation. This is also confirmed by the minor consumption of oxygen in the reactor (ca. 30% conversion). As a consequence, a clear hotspot was not observed for Li/MgO during OCM (Figure 5C). The suppression of highly exothermic reactions at the front of the bed, together with the availability of oxygen throughout the whole catalytic bed, provokes a fundamental change in the catalytic behavior of the Li-promoted system. In fact, while most of the OCM activity was confined to the front or even before the catalyst bed for MgO (Figure 6A−C), the concentration of the C_2 species progressively increased along the Li/MgO catalyst bed.

https://doi.org/10.1021/acssuschemeng.3c02088
ACS Sustainable Chem. Eng. 2023, 11, 10835−10844

For the strontium-doped La_2O_3 (Sr/La_2O_3) system, which showed significant suppression of the partial oxidation products (CO, H_2) compared to La_2O_3, the positive effect of the promoter was less prominent compared to Li/MgO. In fact, consistent formation of water was detected together with the fast depletion of oxygen at the front of the bed (Figures S11 and S6C in the Supporting information).

The unicity of the lithium-promoting effect is associated with the enhancement of catalyst basicity.[38] Such a property was found to be linked to the increased C_2 selectivity.[25] Another effect of Li promotion is the enhancement of the lattice oxygen mobility.[46] Considering the specific selectivity of the lattice oxygen species observed for MgO, their increased mobility in the presence of Li can positively influence the rate of formation of C_2 products. A closer look at the concentration profiles obtained for Li/MgO (Figure 6D) reveals a much higher selectivity to ethane than ethylene. This confirms that the Li-modified surface facilitates the coupling reaction but at the same time does not promote the subsequent oxidative dehydrogenation of ethane (Figure S12). Also to be remarked, during the gas sampling experiment with Li/MgO, the outer surface of the capillary used to extract gases was coated with a material after the experiment, which was not observed for MgO. Loss of Li from the material in the form of LiOH has been reported for Li/MgO as the main cause of deactivation in OCM.[47] This implies a high mobility of the Li component over MgO, which was likely in a molten state under the reaction conditions and adhered to the capillary surface during the gas sampling experiment. This molten state of Li and its ability to cover the MgO support are expected to play an important role in reducing the catalyst surface area and its general catalytic activity. However, we observed that the specific effect of Li promoters is to limit the activity of the MgO lattice oxygen for partial and total oxidation, resulting in increased selectivity toward C_2 formation.

CONCLUSIONS

Simple metal oxides such as MgO and La_2O_3, which possess intrinsically different abilities to selectively convert CH_4, exhibited similar OCM performances in terms of CH_4 conversion and C_2 selectivity at high temperatures.

Space-resolved operando visualization, temperature measurement, and gas sampling along the catalytic bed helped us demonstrate the relevance of highly exothermic reaction paths developed in OCM conditions over those catalysts. The formation of huge hotspots at the front of the catalyst bed derives from a pattern of highly exothermic reactions, including H_2 oxidation. Such hotspots greatly control the total C_2 yield, driving the selectivity toward partial and total oxidation products (CO_x) and narrowing the role of the catalyst to the mere activation of CH_4. The use of promoters, in particular Li on MgO, enhances the control on selectivity by avoiding the formation of hotspots, quenching the unselective oxidation paths and activating the selective conversion to C_2 all along the catalytic bed.

These insights demonstrated the importance of temperature and concentration gradients in the catalytic OCM reaction, stressing the value of implementing spatially resolved analysis for a realistic investigation of the catalytic systems under operating conditions.

ASSOCIATED CONTENT

Supporting Information

The Supporting Information is available free of charge at https://pubs.acs.org/doi/10.1021/acssuschemeng.3c02088.

Schematics of the experimental setup: XRD; additional catalytic activity results, and additional spatial analysis results (PDF)

AUTHOR INFORMATION

Corresponding Author

Atsushi Urakawa − *Catalysis Engineering, Department of Chemical Engineering, Delft University of Technology, 2629 HZ Delft, The Netherlands; Institute of Chemical Research of Catalonia (ICIQ), The Barcelona Institute of Science and Technology, 43007 Tarragona, Spain; Japan Science and Technology Agency (JST), 102-0076 Tokyo, Japan;* orcid.org/0000-0001-7778-4008; Email: A.Urakawa@tudelft.nl

Authors

Lingjun Hu − *Catalysis Engineering, Department of Chemical Engineering, Delft University of Technology, 2629 HZ Delft, The Netherlands; Institute of Chemical Research of Catalonia (ICIQ), The Barcelona Institute of Science and Technology, 43007 Tarragona, Spain*

Donato Pinto − *Catalysis Engineering, Department of Chemical Engineering, Delft University of Technology, 2629 HZ Delft, The Netherlands; Institute of Chemical Research of Catalonia (ICIQ), The Barcelona Institute of Science and Technology, 43007 Tarragona, Spain;* orcid.org/0000-0002-4509-3904

Complete contact information is available at: https://pubs.acs.org/10.1021/acssuschemeng.3c02088

Author Contributions

The manuscript was written through contributions of all authors. All authors have given approval to the final version of the manuscript.

Funding

Financial support by Japan Science and Technology agency (JST) through the PRESTO program (No. JPMJPR16S3) and Generalitat de Catalunya through the CERCA Programme are greatly acknowledged.

Notes

The authors declare no competing financial interest.

REFERENCES

(1) IEA. Global Energy Review: CO_2 Emissions in 2021International Energy AgencyParis, 2022. https://www.iea.org/data-and-statistics/data-product/global-energy-review-CO2-emissions-in-2021#co2-emission-in-2021 (accessed March 01, 2023).

(2) Aasberg-Petersen, K.; Dybkjær, I.; Ovesen, C. V.; Schjødt, N. C.; Sehested, J.; Thomsen, S. G. Natural gas to synthesis gas − Catalysts and catalytic processes. *J. Nat. Gas Sci. Eng.* **2011**, 3, 423−459.

(3) Holmen, A. Direct conversion of methane to fuels and chemicals. *Catal. Today* **2009**, *142*, 2−8.

(4) Schwach, P.; Pan, X.; Bao, X. Direct Conversion of Methane to Value-Added Chemicals over Heterogeneous Catalysts: Challenges and Prospects. *Chem. Rev.* **2017**, *117*, 8497−8520.

(5) Karakaya, C.; Kee, R. J. Progress in the direct catalytic conversion of methane to fuels and chemicals. *Prog. Energy Combust. Sci.* **2016**, *55*, 60−97.

(6) Lunsford, J. H. Catalytic conversion of methane to more useful chemicals and fuels: a challenge for the 21st century. *Catal. Today* **2000**, *63*, 165−174.
(7) Ren, T.; Patel, M.; Blok, K. Olefins from conventional and heavy feedstocks: Energy use in steam cracking and alternative processes. *Energy* **2006**, *31*, 425−451.
(8) Blanksby, S. J.; Ellison, G. B. Bond Dissociation Energies of Organic Molecules. *Acc. Chem. Res.* **2003**, *36*, 255−263.
(9) Franz, R.; Uslamin, E. A.; Pidko, E. A. Challenges for the utilization of methane as a chemical feedstock. *Mendeleev Commun.* **2021**, *31*, 584−592.
(10) Keller, G. E.; Bhasin, M. M. Synthesis of ethylene via oxidative coupling of methane: I. Determination of active catalysts. *J. Catal.* **1982**, *73*, 9−19.
(11) Lunsford, J. H. The Catalytic Oxidative Coupling of Methane. *Angew. Chem., Int. Ed.* **1995**, *34*, 970−980.
(12) Kondratenko, E. V.; Schlüter, M.; Baerns, M.; Linke, D.; Holena, M. Developing catalytic materials for the oxidative coupling of methane through statistical analysis of literature data. *Catal. Sci. Technol.* **2015**, *5*, 1668−1677.
(13) Hu, L.; Pinto, D.; Urakawa, A. Active Reactions and Spatial Gradients in Oxidative Coupling of Methane. In *Catalysis*; The Royal Society of Chemistry, 2020; Vol. *32*, pp 203−223.
(14) Cruellas, A.; Bakker, J. J.; van Sint Annaland, M.; Medrano, J. A.; Gallucci, F. Techno-economic analysis of oxidative coupling of methane: Current state of the art and future perspectives. *Energy Convers. Manage.* **2019**, *198*, No. 111789.
(15) Zavyalova, U.; Holena, M.; Schlögl, R.; Baerns, M. Statistical Analysis of Past Catalytic Data on Oxidative Methane Coupling for New Insights into the Composition of High-Performance Catalysts. *ChemCatChem* **2011**, *3*, 1935−1947.
(16) Nelson, P. F.; Lukey, C. A.; Cant, N. W. Isotopic evidence for direct methyl coupling and ethane to ethylene conversion during partial oxidation of methane over lithium/magnesium oxide. *J. Phys. Chem. A* **1988**, *92*, 6176−6179.
(17) Ito, T.; Watanabe, T.; Tashiro, T.; Toi, K. Reaction of preadsorbed methane with oxygen over magnesium oxide at low temperatures. *J. Chem. Soc., Faraday Trans. 1* **1989**, *85*, 2381−2395.
(18) DeBoy, J. M.; Hicks, R. F. The oxidative coupling of methane over alkali, alkaline earth, and rare earth oxides. *Ind. Eng. Chem. Res.* **1988**, *27*, 1577−1582.
(19) DeBoy, J. M.; Hicks, R. F. Oxidative coupling of methane over alkaline earth promoted La_2O_3. *J. Chem. Soc., Chem. Commun.* **1988**, 982−984.
(20) Choudhary, V. R.; Rane, V. H.; Pandit, M. Y. Comparison of Alkali Metal Promoted MgO Catalysts for Their Surface Acidity/Basicity and Catalytic Activity/Selectivity in the Oxidative Coupling of Methane. *J. Chem. Technol. Biotechnol.* **1997**, *68*, 177−186.
(21) Choudhary, V. R.; Mulla, S. A. R.; Rane, V. H. Surface basicity and acidity of alkaline earth-promoted La_2O_3 catalysts and their performance in oxidative coupling of methane. *J. Chem. Technol. Biotechnol.* **1998**, *72*, 125−130.
(22) Choudhary, V. R.; Rane, V. H.; Chaudhari, S. T. Surface properties of rare earth promoted MgO catalysts and their catalytic activity/selectivity in oxidative coupling of methane. *Appl. Catal., A* **1997**, *158*, 121−136.
(23) Carreiro, J. A. S. P.; Baerns, M. Oxidative coupling of methane: I. Alkaline earth compound catalysts. *J. Catal.* **1989**, *117*, 258−265.
(24) Kalenik, Z.; Wolf, E. E. Transient and isotopic studies of the oxygen transport and exchange during oxidative coupling of methane on Sr promoted La_2O_3. *Catal. Lett.* **1991**, *9*, 441−449.
(25) Arndt, S.; Laugel, G.; Levchenko, S.; Horn, R.; Baerns, M.; Scheffler, M.; Schlögl, R.; Schomäcker, R. A Critical Assessment of Li/MgO-Based Catalysts for the Oxidative Coupling of Methane. *Catal. Rev.* **2011**, *53*, 424−514.
(26) Buyevskaya, O. V.; Rothaemel, M.; Zanthoff, H. W.; Baerns, M. Transient Studies on Reaction Steps in the Oxidative Coupling of Methane over Catalytic Surfaces of MgO and Sm_2O_3. *J. Catal.* **1994**, *146*, 346−357.
(27) Ortiz-Bravo, C. A.; Chagas, C. A.; Toniolo, F. S. Oxidative coupling of methane (OCM): An overview of the challenges and opportunities for developing new technologies. *J. Nat. Gas Sci. Eng.* **2021**, *96*, No. 104254.
(28) Kondratenko, E. V.; Baerns, M. Oxidative Coupling of Methane. In *Handbook of Heterogeneous Catalysis*; Wiley, 2008; pp 3010−3023.
(29) Basile, F.; Fornasari, G.; Trifirò, F.; Vaccari, A. Partial oxidation of methane: Effect of reaction parameters and catalyst composition on the thermal profile and heat distribution. *Catal. Today* **2001**, *64*, 21−30.
(30) Zohour, B.; Noon, D.; Senkan, S. New Insights into the Oxidative Coupling of Methane from Spatially Resolved Concentration and Temperature Profiles. *ChemCatChem* **2013**, *5*, 2809−2812.
(31) Pak, S.; Qiu, P.; Lunsford, J. H. Elementary Reactions in the Oxidative Coupling of Methane over $Mn/Na_2WO_4/SiO_2$ and $Mn/Na_2WO_4/MgO$ Catalysts. *J. Catal.* **1998**, *179*, 222−230.
(32) Otsuka, K.; Jinno, K. Kinetic studies on partial oxidation of methane over samarium oxides. *Inorg. Chim. Acta* **1986**, *121*, 237−241.
(33) Wang, P.; Zhao, G.; Wang, Y.; Lu, Y. $MnTiO_3$-driven low-temperature oxidative coupling of methane over TiO_2-doped Mn_2O_3-Na_2WO_4/SiO_2 catalyst. *Sci. Adv.* **2017**, *3*, No. e1603180.
(34) Fleming, P.; Farrell, R. A.; Holmes, J. D.; Morris, M. A. The Rapid Formation of $La(OH)_3$ from La_2O_3 Powders on Exposureto Water Vapor. *J. Am. Ceram. Soc.* **2010**, *93*, 1187−1194.
(35) Fleischer, V.; Littlewood, P.; Parishan, S.; Schomäcker, R. Chemical looping as reactor concept for the oxidative coupling of methane over a $Na_2WO_4/Mn/SiO_2$ catalyst. *Chem. Eng. J.* **2016**, *306*, 646−654.
(36) Beck, B.; Fleischer, V.; Arndt, S.; Hevia, M. G.; Urakawa, A.; Hugo, P.; Schomäcker, R. Oxidative coupling of methane - A complex surface/gas phase mechanism with strong impact on the reaction engineering. *Catal. Today* **2014**, *228*, 212−218.
(37) Peil, K. P.; Goodwin, J. G.; Marcelin, G. Surface phenomena during the oxidative coupling of methane over Li/MgO. *J. Catal.* **1991**, *131*, 143−155.
(38) Carreiro, J. A. S. P.; Baerns, M. Catalytic conversion of methane by oxidative coupling to C_{2+} hydrocarbons. *React. Kinet. Catal. Lett.* **1987**, *35*, 349−360.
(39) Lin, C. H.; Campbell, K. D.; Wang, J. X.; Lunsford, J. H. Oxidative dimerization of methane over lanthanum oxide. *J. Phys. Chem. A* **1986**, *90*, 534−537.
(40) Rosynek, M. P. Catalytic Properties of Rare Earth Oxides. *Catal. Rev.* **1977**, *16*, 111−154.
(41) Zohour, B.; Noon, D.; Senkan, S. Spatial Concentration and Temperature Profiles in Dual-Packed-Bed Catalytic Reactors: Oxidative Coupling of Methane. *ChemCatChem* **2014**, *6*, 2815−2820.
(42) Karakaya, C.; Zhu, H.; Zohour, B.; Senkan, S.; Kee, R. J. Detailed Reaction Mechanisms for the Oxidative Coupling of Methane over La_2O_3/CeO_2 Nanofiber Fabric Catalysts. *ChemCatChem* **2017**, *9*, 4538−4551.
(43) Sekine, Y.; Nishimura, T.; Fujimoto, K. Oxidative Coupling of Methane in the Gas Phase: Simulation and Reaction Mechanism. *Energy Fuels* **1998**, *12*, 828−829.
(44) Geerts, J. W. M. H.; Chen, Q.; van Kasteren, J. M. N.; van der Wiele, K. Thermodynamics and kinetic modeling of the homogeneous gas phase reactions of the oxidative coupling of methane. *Catal. Today* **1990**, *6*, 519−526.
(45) Takanabe, K.; Iglesia, E. Rate and Selectivity Enhancements Mediated by OH Radicals in the Oxidative Coupling of Methane Catalyzed by $Mn/Na_2WO_4/SiO_2$. *Angew. Chem., Int. Ed.* **2008**, *47*, 7689−7693.
(46) Peil, K. P.; Marcelin, G.; Goodwin, J. G. The Role of Lattice Oxygen in the Oxidative Coupling of Methane. In *Methane Conversion by Oxidative Processes*; Wolf, E. E., Ed.; Springer Netherlands: Dordrecht, 1992; pp 138−167.

https://doi.org/10.1021/acssuschemeng.3c02088
ACS Sustainable Chem. Eng. 2023, 11, 10835−10844

(47) Korf, S. J.; Roos, J. A.; De Bruijn, N. A.; Van Ommen, J. G.; Ross, J. R. H. Lithium chemistry of lithium doped magnesium oxide catalysts used in the oxidative coupling of methane. *Appl. Catal.* **1990**, *58*, 131−146.

https://doi.org/10.1021/acssuschemeng.3c02088
ACS Sustainable Chem. Eng. 2023, 11, 10835−10844